Integrating Traffic Velocity Data into Predictive Energy Management of Plug-in Hybrid Electric Vehicles

Chao Sun[1], Fengchun Sun[1], Xiaosong Hu[2], J. Karl Hedrick[3] and Scott Moura[2]

Abstract— **Recent advances in the traffic monitoring systems have made traffic velocity information accessible in real time. This paper proposes a supervised predictive energy management framework aiming to improve the fuel economy of a power-split plug-in hybrid electric vehicle (PHEV) by incorporating dynamic traffic feedback data. Compared with conventional model predictive control (MPC), an additional supervisory state of charge (SOC) planning level is constructed in this framework. A power balance PHEV model is developed for this upper level to rapidly generate optimal battery SOC trajectories, which are utilized as final state constraints in the MPC level. The proposed PHEV energy management framework is evaluated under three different scenarios: (i) without traffic information, (ii) with static traffic information, and (iii) with dynamic traffic information. Simulation results show that the proposed control strategy successfully integrates dynamic traffic velocity into the PHEV energy management, and achieves 5% better fuel economy compared with when no traffic information is utilized.**

I. INTRODUCTION

Traffic monitoring systems in intelligent transportation systems have matured rapidly in recent years. Real-time flow data is integrated with short-term and long-term knowledge of traffic speeds to dynamically update the velocity estimates. This effort has made it possible to incorporate dynamic traffic flow information into plug-in hybrid electric vehicle (PHEV) energy management, enabling improved fuel economy. This paper systematically integrates real-time traffic flow velocity into the energy management of a power-split PHEV.

In the energy management problem (EMP) of PHEVs, SOC is an important state for determining the optimal power split ratio between the engine and battery. If no future driving information is available, the charge depleting and charge sustaining (CDCS) strategy is often used [1]. However, given more information about the velocity profile – enabled from traffic data – we hypothesize that a near-optimal energy management strategy can be developed through SOC planning. The authors of [2] developed a SOC reference generator for hilly driving profiles, and demonstrated improved fuel economy. In this paper, we consider a SOC pre-planning approach under time-varying traffic conditions. Real-time traffic data is utilized for SOC planning and control. Meanwhile, vehicle velocities are continuously monitored and fed back into the traffic monitoring system.

MPC controllers for the EMP of PHEVs have been studied for years [3], [4]. However, to the authors' best knowledge, the incorporation of dynamic traffic data into MPC energy management for PHEVs has not been investigated. In this paper, a real-world highway driving scenario is constructed based on real collected traffic flow data from the Mobile Century project [5] as a case study.

The main contribution of this paper is a traffic data enabled predictive control framework for PHEV energy management, to achieve near optimal fuel consumption. Compared with conventional MPC, this framework includes a higher supervisory battery SOC planning level, aiming to improve the controller performance from a global perspective. A power balance PHEV model is developed for reference SOC trajectory generation based on the obtained traffic data. Compared with conventional PHEV models, the power balance model significantly reduces SOC trajectory computation time, thereby enabling real-time implementation at updates rates commensurate with traffic data. A real-world highway driving scenario is used for validation based on the traffic flow data from Mobile Century [5]. Although the foregoing contributions are made specifically for a power-split PHEV in a highway driving scenario, the proposed approach extends directly to other HEV/PHEV configurations or other driving situations when traffic velocity information is available.

The remainder of the paper is arranged as follows. In Section II, the obtained traffic data is presented and analyzed. Section III introduces the supervised predictive energy management strategy. Section IV gives the control-oriented PHEV model and formulates the nonlinear control problem. Simulation results are illustrated in Section V, followed by key conclusions in Section VI.

II. TRAFFIC FLOW VELOCITY ANALYSIS

Reference [5] presents a traffic monitoring system based on GPS-enabled smartphones. This system exploits the extensive coverage of the cellular network, position and velocity measurements of GPS, and the communication infrastructure of cellphones. A field experiment was conducted to measure the velocity of traffic flow on a 10-mile stretch of I-880 near Union City, California, for 8 hours. The data is used for the PHEV energy management study in this paper.

Vehicle in the experiment were all equipped with GPS-enabled mobile devices, which can produce time-stamped position and velocity measurements every 3 seconds. A traffic estimation server is used to collect all the GPS data

[1]Chao Sun and Fengchun Sun are with Department of Mechanical and Vehicle Engineering, Beijing Institute of Technology, 100081 Beijing, China chaosun.email@gmail.com, sunfch@bit.edu.cn

[2]Xiaosong Hu and Scott Moura are with Department of Civil and Environmental Engineering, University of California, Berkeley, 94720 CA, USA xiaosonghu@berkeley.edu, smoura@berkeley.edu

[3]Karl Hedrick is with Department of Mechanical Engineering, University of California, Berkeley, 94720 CA, USA khedrick@me.berkeley.edu

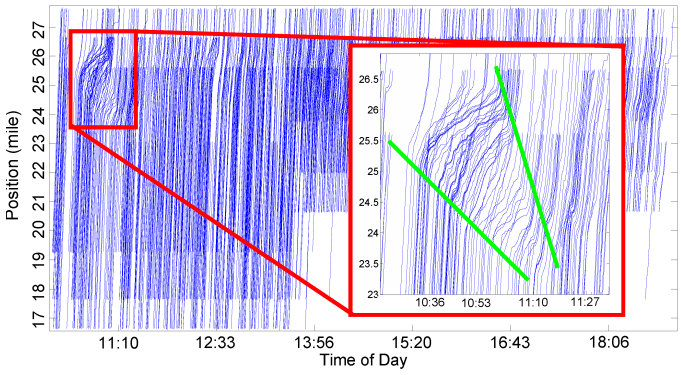

Fig. 1. Collected driving trips from field experiment of Mobile Century. Each blue line represents the trajectory of one collected trip during a day. The positions of each vehicle are identified by post-miles of highway I-880, from 16 to 28 mile northbound.

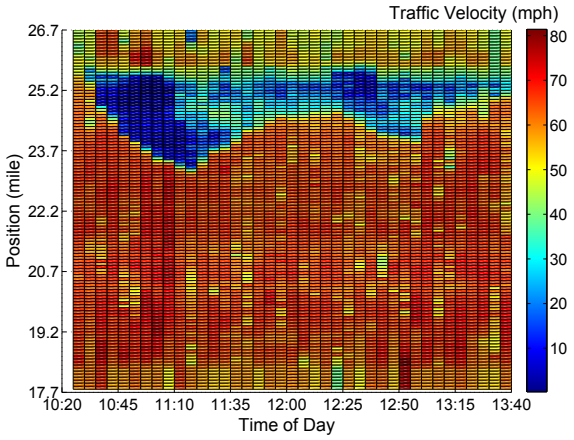

Fig. 2. Traffic flow velocity distribution from 10:20 to 13:40. Sampling time interval is 300 seconds and the road resolution is 0.1 mile.

and analyze traffic flow dynamics. A time-position map can be plotted with the driving trips provided by field experiments of Mobile Century, as illustrated in Fig. 1. A traffic congestion event can be seen from the red rectangle marked in this figure. All vehicles were forced to decelerate when driving through the congestion area. As the influence of the congestion attenuated, the vehicles gradually accelerated back to normal speeds. The propagation of the shock-wave can be observed clearly.

The traffic congestion period, from 10:20 to 13:40 is selected deliberately as the object of study. The trip data is assumed to be collected and analyzed by a central server. The traffic flow velocity distribution is computed and the vehicle can obtain it via the Internet. Note that the flow velocity data received by the drivers is only a static reflection of the traffic. The information is more valuable when it updates in real-time. In this paper, we assume the driver can obtain the traffic flow data every 300 seconds, which is consistent with the update rate of the Caltrans Performance Measurement Systems (PeMS) [6].

The extracted traffic flow velocity is demonstrated in Fig. 2. As can be seen, the flow velocity reduces greatly from 70 mph to less than 10 mph near the 24-mile position, 10:45

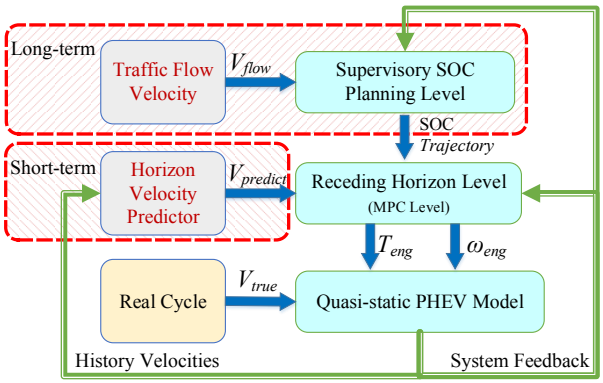

Fig. 3. The proposed supervised predictive energy management for PHEVs, assuming that the terrain information is pre-stored in a 3D map.

AM. The velocity of the congestion part starts to increase from about 11:20 AM. The traffic flow velocity is assumed to be the real driving profile that the target vehicle will drive along. However, due to the fact that the road resolution is low, the extracted traffic velocity profile is piecewise constant. We smooth this data with a Butterworth filter to produce a more realistic and trackable velocity signal.

III. SUPERVISED PREDICTIVE ENERGY MANAGEMENT

A. *Traffic Enabled Energy Management*

The structure of the dynamic traffic enabled predictive energy management is demonstrated in Fig. 3. The traffic flow velocity V_{flow} used by the supervisory SOC planning level is utilized for long-term optimal SOC trajectory calculation. A horizon velocity predictor is employed to forecast short-term future driving velocities in each receding horizon. As such, the upper and lower-levels correspond to the long-term and short-term disturbances, respectively.

The SOC trajectory is introduced into the MPC level as a terminal reference during each horizon. This provides the lower level MPC feedback loop with additional control flexibility to compensate for SOC errors, denoted as

$$\overline{\mathrm{SOC}}(t) \quad = \quad \mathrm{SOC}^*(t) \tag{1}$$

where $\overline{\mathrm{SOC}}$ is the terminal SOC reference for the MPC level and SOC^* is the generated optimal SOC trajectory from the supervisory SOC planning level. The general control procedure is described as below, to be elaborated in the following sections:

- Acquire the traffic and route information, calculate the reference SOC trajectory;
- Predict the short-term future velocity profile via the horizon velocity predictor;
- Given the SOC reference and forecasted short-term velocity, calculate the control policies in MPC level;
- Apply the first element of the optimal control policy, feedback and repeat.

Note that the upper and lower levels utilize different PHEV models for optimization. In the upper level, a simple power-based model is utilized for SOC trajectory generation. In the

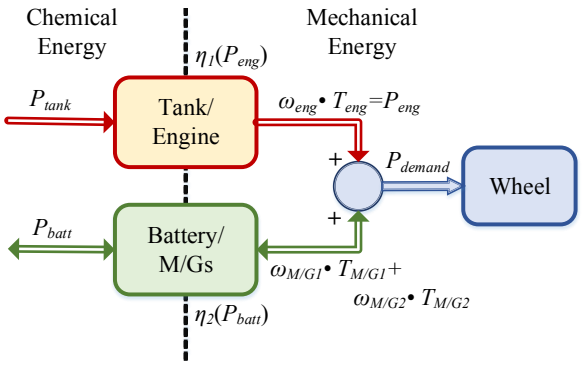

Fig. 4. Power flow topology for the power-split PHEV powertrain.

lower level, a higher fidelity PHEV model is used for MPC. We describe each level in the following subsections. The quasi-static PHEV model is a detailed plant model furnished by the QSS-toolbox developed at ETH, which has been validated against experiments (see [7] for details).

B. Long-term SOC Trajectory Generation

The reference SOC trajectory calculation must be fast enough to follow the traffic dynamics. The commonly used control-oriented PHEV model [8] is proficient for powertrain control, but excessively complex for SOC trajectory calculation for this particular purpose. This paper introduces a reduced power balance based model, which is much more computationally efficient, yet sufficiently accurate for the purpose of SOC trajectory generation.

The power balance model is based on the power flow in Fig. 4, which describes power flows and conversion efficiencies. The tank/engine converts chemical energy into mechanical energy with efficiency denoted by η_1. The battery and two motor/generators (M/Gs) convert between chemical battery energy and mechanical energy with efficiency denoted by η_2. The sum of the engine and M/Gs' mechanical powers must equal power demand, P_{demand}. Mathematically, the simplified powertrain is governed by power balance equation

$$\eta_1 P_{tank}(t) + \eta_2 P_{batt}(t) = P_{demand}(t) \tag{2}$$

where P_{tank} is the chemical energy supplied by the tank, P_{batt} is the electro-chemical energy supplied by the battery and P_{demand} is the vehicle power demand. Positive P_{batt} denotes discharging. Parameters η_1 and η_2 are synthetic energy conversion coefficients of the mechanical propulsion path (engine side) and the electrical propulsion path (M/G side), respectively. The power demand is provided by

$$P_{demand}(t) = \left(ma(t) + C_r mg + \frac{1}{2}\rho A C_d v^2(t) \right) v(t) \tag{3}$$

where m is the vehicle mass, $a(t)$ is the vehicle acceleration, g is gravitational acceleration, $v(t)$ is the vehicle velocity, C_r represents the rolling resistance coefficient and $\frac{1}{2}\rho A C_d$ is the aerodynamic drag resistance. Note that the wheel inertia is neglected and the road grade is assumed to be zero in this paper. The battery pack is modeled as an equivalent circuit [9]. The battery power and SOC are modeled as

$$P_{batt}(t) = V I_{batt}(t) - I_{batt}^2(t) R \tag{4}$$

$$\dot{\text{SOC}}(t) = -\frac{I_{batt}(t)}{Q} \tag{5}$$

where V and R are the open circuit voltage and internal resistance, respectively; $I_{batt}(t)$ and Q are the battery current and capacity, respectively.

In this power balance model, the number of control variables is reduced from two to one compared with the control-oriented model (presented in [10]). Battery output power is selected as the control variable, where $u = P_{batt}$. Battery SOC and the engine on/off state (denoted as O) are selected as state variables, where $x = [\text{SOC}, \text{O}]^T$. $\text{O} = 1$ means the engine is on, and $\text{O} = 0$ means the engine is off. Define switching of the engine state as

$$\delta\text{O}(k\Delta t) = |\text{O}(k\Delta t) - \text{O}((k-1)\Delta t)| \tag{6}$$

The cost function is formulated as

$$J = \int_0^T \left[P_{tank}(u(t)) + w \cdot \delta\text{O}(t) \right]^2 dt \tag{7}$$

where $P_{tank}(u(t))$ penalizes fuel consumption and w is the penalty for engine state switching. The expression for $P_{tank}(u(t))$ is derived as follows. From (2) we have

$$P_{tank}(t) = \frac{P_{demand}(t) - \eta_2 P_{batt}(t)}{\eta_1}. \tag{8}$$

Note that $u(t) = P_{batt}(t)$. Moreover, consider the conversion efficiencies with the following arguments

$$\eta_1 = \eta_1(P_{eng}), \tag{9}$$

$$\eta_2 = \eta_2(P_{batt}) = \eta_2(u). \tag{10}$$

Note that $P_{eng} = P_{demand} - \eta_2 P_{batt} = P_{demand} - \eta_2(u) \cdot u$. Consequently, we obtain

$$P_{tank}(t) = \frac{P_{demand}(t) - \eta_2(u(t)) \cdot u(t)}{\eta_1(P_{eng}(t))} = \frac{P_{eng}(t)}{\eta_1(P_{eng}(t))}. \tag{11}$$

Dynamic Programming (DP) is used to minimize J, subject to constraints

$$\text{SOC}^{\min} \le \text{SOC} \le \text{SOC}^{\max},\ P_{tank}^{\min} \le P_{tank} \le P_{tank}^{\max};$$
$$I_{batt}^{\min} \le I_{batt} \le I_{batt}^{\max},\ P_{batt}^{\min} \le P_{batt} \le P_{batt}^{\max}.$$

Efficiencies η_1, η_2 for this power balance model are determined empirically. Namely, η_1 can be calculated by assuming the engine always operates on the optimum operating line (OOL). In contrast, η_2 involves the combined operating efficiencies of both M/G1 and M/G2, and it is therefore not possible to assume operation along the individual OOLs. Thus, this paper proposes an empirical approach to determine η_1 and η_2, based on the optimal operating behaviors yielded from the control-oriented model. Details are shown below:

- First, utilize DP to solve the EMP with the control-oriented PHEV model across a variety of driving cycles;

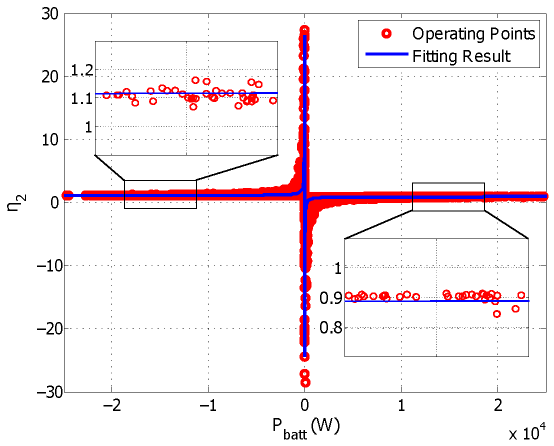

Fig. 5. The P_{batt}-η_2 operating points and the curve fitting result.

- Second, collect the optimal solutions for powertrain behavior analysis. Coefficients η_1 and η_2 are calculated by

$$\eta_1 = \frac{\omega_{eng} \cdot T_{eng}}{P_{tank}} \quad (12)$$

$$\eta_2 = \frac{\omega_{M/G1} \cdot T_{M/G1} + \omega_{M/G2} \cdot T_{M/G2}}{P_{batt}} \quad (13)$$

  where ω_{eng}, $\omega_{M/G1}$, $\omega_{M/G2}$ and T_{eng}, $T_{M/G1}$, $T_{M/G2}$ are corresponding rotation speeds and torques of the engine, M/G1 and M/G2.
- Last but most important, formulate η_1 and η_2 by least squares curve fitting.

In step one, four driving cycles, including both urban and highway types, are used for the optimal energy management simulation: WVUCITY, NYCC, Artemis-highway and HWFET. Different battery discharging depths are also investigated. The operating points for function η_2 are plotted in Fig. 5. It can be seen that η_2 is strongly correlated with P_{batt}. Consequently, the hypotheses in (9) and (10) are verified. Interestingly, the fitting results for η_1 prove to be consistent with the engine OOL approach. Piecewise functions are employed for curve fitting of η_2, including polynomial functions and mixture Gaussian functions.

The complete power balance-based model is validated in Section V-A against a more detailed control-oriented model. Next we consider the issue of velocity prediction in the MPC level from Fig 3.

C. Short-term Velocity Prediction

Next we develop a forecasting technique to predict short-term vehicle velocities. This paper employs a data driven approach to velocity prediction. Vehicles with forward radar devices can utilize lead vehicle measurements to improve velocity prediction, but this is not considered here.

In recent work on velocity prediction [11], artificial neural networks (ANN) have proven effective in terms of both accuracy and ease-of-use. Here, a radial basis function neural network (RBF-NN) based velocity predictor is selected for short-term velocity prediction, based on a velocity predictor comparison study in [12]. The input of the RBF-NN predictor is a historical velocity sequence, and the output is short-term future velocity sequence $V_{predict}$. Four standard driving cycles are used for the network training, including both highway and urban types: UDDS, HWFET, NEDC, US06. A real driving cycle is selected for validation from the highway driving data collected from Mobile Century. According to the empirical cumulative distribution function (CDF) of the root-mean-square errors (RMSE) of all the prediction processes, nearly 90% of the RMSEs are below 1.5 m/s. Therefore, we conclude that the RBF-NN velocity predictor is accurate enough for MPC-based PHEV energy management. Note that other velocity prediction methods, such as Gaussian mixture modeling or stochastic approaches, could also be implemented in this part.

IV. CONTROL FORMULATION IN MPC

The control-oriented power-split PHEV powertrain model is deployed in the MPC level. For brevity, this paper omits the equations of the model. The details and notation information of the PHEV mpowertrain model can be found in [10].

The EMP in the MPC level is formulated as a constrained nonlinear optimization problem and solved by DP. Given the powertrain dynamics in [10], ω_{eng} and T_{eng} are chosen as control variables. Denoting x as the state variable, u as the control variable, d as the system disturbance, and y as the output, the proposed control-oriented powertrain model can be represented as

$$\begin{aligned} \dot{x} &= f(x,u,d) \\ y &= g(x,u,d) \end{aligned} \quad (14)$$

with $x = [\text{SOC}, \text{O}]^T$, $u = [\omega_{eng}, T_{eng}]^T$, $d = V_{predict}$, $y = \left[\dot{m}_{fuel}, P_{batt}, T_{M/G2}, \omega_{M/G1}, T_{M/G1}\right]^T$. Consider a one second time step, $\Delta t = 1$ second. At time step k, the cost function J_k is formulated as

$$J_k = \int_{k\Delta t}^{(k+H_p)\Delta t} \left[\dot{m}_{fuel}(u(t)) + w\delta\text{O}(t)\right]^2 \, dt \quad (15)$$

where H_p is the prediction horizon length, which is herein equal to the control horizon length for simplicity. The disturbance $d = V_{predict}$ is predicted by the short-term velocity predictor in Section III-C. Additionally, the physical constraints for SOC, I_{batt}, P_{batt}, T_{eng}, ω_{eng}, $T_{M/G1}$, $\omega_{M/G1}$, $T_{M/G2}$, and $\omega_{M/G2}$ must be enforced.

The terminal battery SOC constraint in the MPC horizon must also be verified, as given by the SOC trajectory generated from the traffic flow data. Note the SOC reference can be indexed in two ways: over a time domain and over a space domain. For a time domain dependent SOC reference,

$$\overline{\text{SOC}}((k+H_p)\Delta t) = \text{SOC}^*((k+H_p)\Delta t) \quad (16)$$

For a space domain dependent SOC reference,

$$\overline{\text{SOC}}(n_k \Delta s) = \text{SOC}^*(n_k \Delta s) \quad (17)$$

where Δs is the space step, n_k indicates the space step number that the vehicle drives through by the end of time

horizon k. SOC* is the optimal SOC trajectory generated from the supervisory SOC planning level in Section III-B. Both of these two index options are investigated in the following section.

V. SIMULATION AND DISCUSSION

All the simulations were performed on a computer with an Intel Corel i7-3630QM CPU @2.4GHz. The power-split PHEV structure and parameters are also adopted from [10]. Note that in the simulation, we focus on trips that exceed the all-electric-range, and require engine power at some point.

A. Power Balance Model Validation

The power balance model is validated by comparing the generated SOC trajectory with the control-oriented model. The optimization problem (7) and (15) are all solved by DP with the same discretization resolution. The initial battery SOC is set as 0.7 and terminal SOC is set as 0.3. Six standard driving cycles and two real-world cycles, highway-$Real_h$ and urban-$Real_u$, are combined arbitrarily to construct three longer trips for testing. Note that the validation driving cycles are different from those used to identify η_1 and η_2. Details of the trips are shown in the top of Table I.

The bottom of Table I reports a comparison of SOC trajectory generation from the two PHEV models: higher-fidelity control oriented (C.O) versus lower-fidelity power balance (P.O). Symbol T is the computation time. The control oriented model requires 190-260 seconds to compute the SOC trajectory. It may be difficult for this model to satisfy the real-time traffic information updating requirement on an embedded system. However, the computation time required by the power balance model is 80% less than the control-oriented model (30-40 seconds). The power balance model facilitates real-time SOC trajectory production, and is computationally sufficient for rapid SOC trajectory calculation. Denote the SOC error as $e(t)$, thus,

$$e(t) = \text{SOC}_p(t) - \text{SOC}_c(t) \tag{18}$$

where $\text{SOC}_p(t)$ and $\text{SOC}_c(t)$ are the SOC trajectories calculated from the power balance model and the control-oriented model, respectively. It can be seen that the average and maximal SOC errors over time of the power balance model remain within 3% and 5% of the battery SOC full scale, respectively. This demonstrates that the power balance model is reasonably accurate for the reference SOC trajectory calculation, and therefore serves the SOC planning purpose at the top level of Fig. 3. The resultant battery SOC trajectories of the 3/Mixed driving trip testing are illustrated in Fig. 6. As can be seen, the SOC trajectory of the power balance model follows the control-oriented model well.

B. Energy Management Strategy Evaluation

The congestion period from 10:20 to 13:40 in the Mobile Century data is chosen to evaluate the proposed energy management strategy. Six arbitrarily selected driving trips are used for testing. Each testing cycle includes one or two traffic congestions. The SOC reference is computed simultaneously

TABLE I
TRIP DETAILS & SOC TRAJECTORY COMPARISON

Trip No./Type	Composed by Cycles	Length (s/km)
1/Urban	UDDS NEDC $Real_u$	3528/32.8
2/Highway	HWFET WVUINTER $Real_h$	4112/65.0
3/Mixed	WVUSUB US06 $Real_h$ $Real_u$	4820/56.3

Trip No./Model	Avg $\lvert e\rvert$	Max $\lvert e\rvert$	T (s)	SOC
1/C.O.	—	—	197.2 (100%)	0.30
1/P.B.	0.0147	0.0249	31.8 (16.1%)	0.30
2/C.O.	—	—	231.9 (100%)	0.30
2/P.B.	0.0226	0.0467	37.5 (16.2%)	0.30
3/C.O.	—	—	261.1 (100%)	0.30
3/P.B.	0.0168	0.0438	41.2 (15.8%)	0.30

'C.O.' and 'P.B.' denote the control-oriented model and the power balance model, respectively. SOC denotes the terminal SOC value.

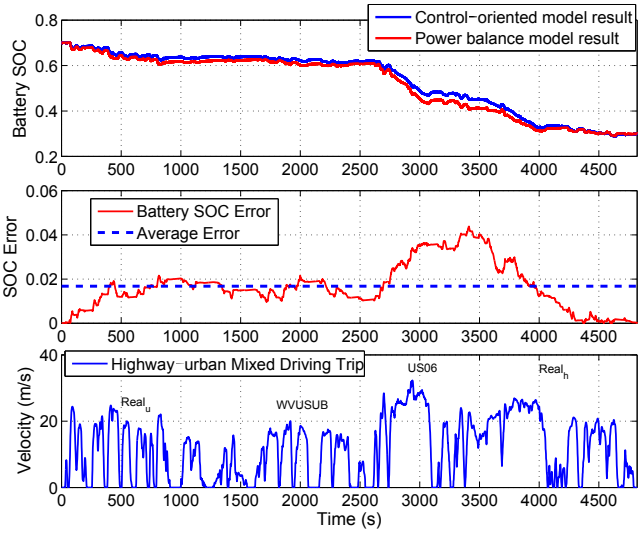

Fig. 6. Comparison of SOC trajectory in the 3/Mixed case. From top to bottom: SOC trajectories, the absolute SOC error $|e|$ and the driving profile. The average $|e|$ is 0.0168 (1.68% of the battery SOC full scale).

during the simulation. All of the real driving profiles are completely blind to all the MPC simulations. The same RBF-NN velocity predictor is used for short-term velocity prediction. For simplicity, the control and prediction horizons are both set as 10 steps, as a compromise between control performance and computational complexity. The average computation time of the simulation process at each time instant (one second) is 0.6-0.7 seconds, which is potentially implementable on an embedded system.

Based on different traffic data accessibility levels, five situations are considered to evaluate the proposed supervised predictive energy management strategy:

1) **CDCS:** When no traffic information is available, the CDCS strategy is used for battery SOC planning.
2) **Static@T:** Static traffic information is available and the vehicle obtains traffic information only at beginning of the trip, with SOC reference indexed by time.
3) **Static@S:** Static traffic information is available and the SOC reference is indexed by space.

TABLE II

SIMULATION RESULTS FOR TRIP 2

Type	Terminal SOC	Fuel$_c$ (g)	Fuel Optimality
DDP	0.3000	628.5	100%
CDCS	0.2955	691.6	89.9%
Static@T	0.3911	712.2	86.7%
Static@S	0.2965	678.9	92.0%
Dynamic@T	0.2895	659.1	95.1%
Dynamic@S	0.2971	654.5	95.9%

DDP means deterministic DP, where full knowledge of the driving cycle is known in a prior and DP computes the optimal solution in theory.

4) **Dynamic@T:** Dynamic traffic information is available every 300 seconds. The SOC is indexed by time.
5) **Dynamic@S:** Dynamic traffic information is available, and the SOC reference is indexed by space.

The deviation between the final battery SOC and the desired value has been compensated in the fuel consumption calculations, denoted as Fuel$_c$. Detailed simulation results for one of the testing trips are listed in Table II, including deterministic DP as a benchmark. As expected, the fuel consumption of predictive energy management with dynamic traffic information available is less than the CDCS strategy and the static traffic information approaches.

Simulation results for all six testing trips are illustrated in Fig. 7, including the average value and standard deviation of the fuel optimality and the terminal SOC. The CDCS maintains an average of 90% fuel optimality, and the terminal SOC is always restrained around 0.3. Due to utilizing static traffic flow information that poorly predicts traffic evolution, the Static@T performs worse than the CDCS on average. In particular, the terminal SOC has a relatively high variance around 0.3. By indexing the SOC reference in space, Static@S guarantees the terminal SOC constraint is respected with low variance. As a result, the overall fuel economy is improved by 5% on average.

In the Dynamic@T case, the deviation of the terminal SOC is reduced by updating the traffic data frequently compared with the Static@T. The terminal SOC is restricted within an acceptable range between 0.3 and 0.35. More importantly, nearly 94% average fuel optimality is achieved with dynamic traffic enabled, which is a considerable improvement considering the uncertainty of the driving schedules.

The demonstrated results are conducted under a congested highway driving scenario constructed from [5]. Different results could be observed under different traffic conditions. However, the proposed predictive energy management proves effective in achieving near optimal fuel economy with integrated dynamic traffic feedback data.

VI. CONCLUSIONS

This paper presents a predictive PHEV energy management strategy, which integrates real-time traffic flow velocity data. The strategy is with a two-layer hierarchical structure. In the supervisory level, the optimal SOC trajectory is rapidly generated from the dynamic traffic data, which is used as terminal SOC constraints in the lower MPC level. A power balance PHEV model is developed for this upper-level SOC calculation. With this model, DP computes the optimal SOC trajectory in real-time - at a rate commensurate with traffic data update rates (300 sec). Simulation results show that the predictive energy management strategy with dynamic traffic data can achieve 94-96% fuel optimality of the deterministic DP benchmark in a highway driving scenario, despite congestion events. Future work is to validate the proposed energy management strategy via hardware-in-the-loop experiments.

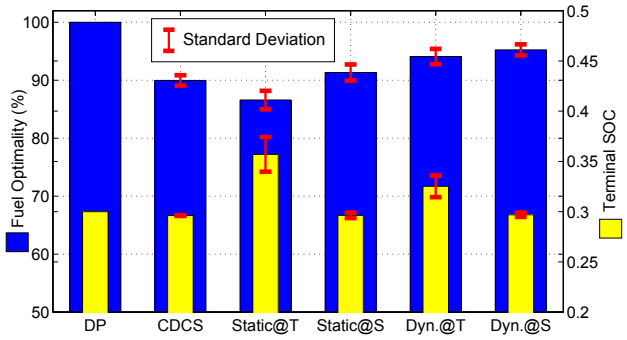

Fig. 7. Average fuel optimality and terminal SOC results for all the testing trips. Dynamic traffic information allows the proposed energy management strategy to achieve nearly 95% fuel optimality while consistently ensuring the terminal SOC value.

REFERENCES

[1] P. Tulpule, V. Marano, and G. Rizzoni, "Effects of different PHEV control strategies on vehicle performance," in *American Control Conference*. IEEE, 2009, pp. 3950–3955.

[2] D. Ambuhl and L. Guzzella, "Predictive reference signal generator for hybrid electric vehicles," *IEEE Transactions on Vehicular Technology*, vol. 58, no. 9, pp. 4730–4740, 2009.

[3] A. Sciarretta and L. Guzzella, "Control of hybrid electric vehicles," *IEEE Control systems*, vol. 27, no. 2, pp. 60–70, 2007.

[4] K. Uthaichana, S. Bengea, R. DeCarlo, S. Pekarek, and M. Zefran, "Hybrid model predictive control tracking of a sawtooth driving profile for an HEV," in *American Control Conference*. IEEE, 2008, pp. 967–974.

[5] J. C. Herrera, D. B. Work, R. Herring, X. J. Ban, Q. Jacobson, and A. M. Bayen, "Evaluation of traffic data obtained via GPS-enabled mobile phones: The mobile century field experiment," *Transportation Research Part C: Emerging Technologies*, vol. 18, no. 4, pp. 568–583, 2010.

[6] C. Chen, K. Petty, A. Skabardonis, P. Varaiya, and Z. Jia, "Freeway performance measurement system: mining loop detector data," *Transportation Research Record: Journal of the Transportation Research Board*, vol. 1748, no. 1, pp. 96–102, 2001.

[7] L. Guzzella and A. Amstutz, "CAE tools for quasi-static modeling and optimization of hybrid powertrains," *IEEE Transactions on Vehicular Technology*, vol. 48, no. 6, pp. 1762–1769, 1999.

[8] J. Liu and H. Peng, "Modeling and control of a power-split hybrid vehicle," *IEEE Transactions on Control Systems Technology*, vol. 16, no. 6, pp. 1242–1251, 2008.

[9] X. Hu, S. Li, and H. Peng, "A comparative study of equivalent circuit models for Li-ion batteries," *Journal of Power Sources*, vol. 198, pp. 359–367, 2012.

[10] S. J. Moura, H. K. Fathy, D. S. Callaway, and J. L. Stein, "A stochastic optimal control approach for power management in plug-in hybrid electric vehicles," *IEEE Transactions on Control Systems Technology*, vol. 19, no. 3, pp. 545–555, 2011.

[11] S. Lefvre, C. Sun, R. Bajcsy, and C. Laugier, "Comparison of parametric and non-parametric approaches for vehicle speed prediction," in *American Control Conference*. IEEE, 2014, pp. 3494–3499.

[12] C. Sun, X. Hu, S. Moura, and F. Sun, "Velocity predictors for predictive energy management in hybrid electric vehicles," *IEEE Transactions on Control System and Technology*, accepted.